

Adaptive Gradient Calibration for Single-Positive Multi-Label Learning in Remote Sensing Image Scene Classification

Chenying Liu , Graduate Student Member, IEEE, Gianmarco Perantoni , Graduate Student Member, IEEE, Lorenzo Bruzzone , Fellow, IEEE, and Xiao Xiang Zhu , Fellow, IEEE

Abstract—Multi-label classification (MLC) offers a more comprehensive semantic understanding of Remote Sensing (RS) imagery compared to traditional single-label classification (SLC). However, obtaining complete annotations for MLC is particularly challenging due to the complexity and high cost of the labeling process. As a practical alternative, single-positive multi-label learning (SPML) has emerged, where each image is annotated with only one relevant label, and the model is expected to recover the full set of labels. While scalable, SPML introduces significant supervision ambiguity, demanding specialized solutions for model training. Although various SPML methods have been proposed in the computer vision domain, research in the RS context remains limited. To bridge this gap, we propose Adaptive Gradient Calibration (AdaGC), a novel and generalizable SPML framework tailored to RS imagery. AdaGC adopts a gradient calibration (GC) mechanism with a dual exponential moving average (EMA) module for robust pseudo-label generation. We introduce a theoretically grounded, training-dynamics-based indicator to adaptively trigger GC, which ensures GC’s effectiveness by preventing it from being affected by model underfitting or overfitting to label noise. Extensive experiments on two benchmark RS datasets under two distinct label noise types demonstrate that AdaGC achieves state-of-the-art (SOTA) performance while maintaining strong robustness across diverse settings. The codes and data will be released at <https://github.com/rslab-unitrento/AdaGC>.

Index Terms—Early learning, gradient calibration (GC), multi-label classification (MLC), noisy labels, Sentinel-1, Sentinel-2, single-positive multi-label learning (SPML), very-high resolution (VHR), weak supervision, remote sensing

I. INTRODUCTION

WITH the rapid development of satellite missions, vast amounts of remote sensing (RS) imagery have become increasingly accessible, serving as a critical data source for numerous applications [1], [2]. Image classification [3]–[5], a fundamental task to connect RS imagery with downstream applications, still largely adopts the single-label classification (SLC) paradigm. However, assigning a single label to each image oversimplifies the complexity of real-world RS scenes [6], [7]. In practice, RS images often contain diverse land cover types, objects, or functional zones. As illustrated in Fig. 1, both

Chenying Liu and Gianmarco Perantoni contributed equally to this work.
(Corresponding authors: Lorenzo Bruzzone; Xiao Xiang Zhu.)

Chenying Liu and Xiao Xiang Zhu are with the Chair of Data Science in Earth Observation, Technical University of Munich (TUM), and Munich Center for Machine Learning (MCML), 80333 Munich, Germany (e-mail: chenying.liu@tum.de; xiaoxiang.zhu@tum.de).

Gianmarco Perantoni and Lorenzo Bruzzone are with the Department of Information Engineering and Computer Science, University of Trento, 38123 Trento, Italy (e-mail: gianmarco.perantoni@unitn.it; lorenzo.bruzzone@unitn.it).

This work has been submitted to the IEEE for possible publication. Copyright may be transferred without notice, after which this version may no longer be accessible.



Fig. 1. Single- and multi-label annotation examples from (a) AID-multilabel [11] and (b) refined BigEarthNet [12] datasets, where the corresponding CLC mask is presented for reference. Compared to the single-class labels, the multi-label annotations can more comprehensively describe the scene.

VHR and lower-resolution imagery commonly capture heterogeneous content, making multi-label classification (MLC) a more informative representation than SLC.

A key challenge for MLC is the difficulty and cost of acquiring complete, accurate annotations [8], especially in the deep learning (DL) era where large-scale labeled datasets are crucial [9]. A practical workaround is to annotate only one relevant label per image, leading to the single-positive multi-label learning (SPML) setting [10]. In this setting, the model is weakly supervised with one positive label per image, yet it is expected to recover the complete set of relevant labels. The supervision in SPML is characterized by missing labels. In practice, even expert annotators often miss relevant labels, making the false negative issue pervasive in MLC. SPML can thus be viewed as an extreme case of this problem.

Although SPML is promising in scalability and annotation efficiency, it introduces significant ambiguity. A common baseline approach is the Assume Negative (AN) strategy [10], which treats all unobserved labels as negatives, unavoidably introducing bias into learning. In the computer vision (CV) domain, several strategies have been proposed to address its limitations, such as noise-robust regularization terms, online label-correction/pseudo-labeling methods, and interpretability-driven frameworks [10], [13]–[18]. Despite the advancements in CV, the SPML problem remains underexplored in RS. SPML is particularly valuable for RS image classification, where annotation typically requires greater domain expertise and incurs higher costs. These challenges make the application of SPML in RS more necessary and also more difficult.

When directly applying existing SPML methods to RS data, several challenges arise. One major issue is the reliability of pseudo-labels. very-high resolution (VHR) RS images often include small, sparsely distributed targets, while medium-to-low-resolution imagery tends to capture broader regional

semantics. Both cases can easily result in low inter-class separability and high intra-class variability, hindering the effectiveness of simple pseudo-labeling strategies such as confidence thresholding. Furthermore, the distinct characteristics of MLC versus multi-class classification (MCC) suggest that commonly used learning-from-noisy-labels strategies, which are often designed for MCC, should be carefully tailored to SPML. Moreover, most existing pseudo-label-based SPML methods depend on fixed warm-up schedules, which often result in suboptimal performance due to model underfitting or overfitting to label noise.

In this work, we propose a novel and generalizable framework for SPML in RS, termed Adaptive Gradient Calibration (AdaGC), to address the aforementioned challenges. The framework consists of three key components. First, we propose a theoretically grounded Gradient Calibration (GC) mechanism designed specifically for SPML. GC aims to alleviate the model's tendency to overfit false negatives by correcting gradients using pseudo-label guidance. Unlike Early Learning Regularization (ELR) [19], which is formulated for multi-class classification under the simplex constraint, GC is rigorously extended to the SPML setting without such a constraint. Second, to guarantee pseudo-label quality, we introduce a dual exponential moving average (EMA) module for robust pseudo-label estimation, which leverages the consensus between the temporally smoothed predictions of the student model and the teacher model's outputs. The former applies EMA to predictions, and the latter to model weights. Then, to ensure the effectiveness of GC, we conduct an in-depth analysis of learning dynamics in SPML and propose a theoretically grounded indicator for adaptive activation of Gradient Calibration (GC) after an initial warm-up stage. This mechanism is central to our design, which is capable of preventing interference from underfitting or noise-driven overfitting to stabilize optimization. We also incorporate the Mixup data augmentation technique [13] within GC to further improve model's generalizability. Extensive experiments on two benchmark RS multi-label datasets demonstrate the effectiveness and robustness of AdaGC.

The main contributions of this paper are summarized as follows:

- We propose a two-stage RS SPML framework, which incorporates an early learning detection strategy to guide the activation of GC to combat underfitting and overfitting to label noise. The theoretical analyses are also provided to support the effectiveness of the framework design.
- We introduce a dual-EMA pseudo-label generation strategy that enhances label completeness and reliability by leveraging temporal prediction fusion.
- We conduct extensive experiments on two benchmark RS datasets covering both high- and low-resolution imagery. For low-resolution data, we employ *Random* and *Dominant* SPML noise simulations to better reflect real-world annotation behavior. For high-resolution imagery, where identifying a dominant class is inherently difficult, we rely on *Random* simulation supplemented with additional *Manual* single-positive annotations. We provide a comprehensive benchmarking of existing SPML methods,

offering valuable insights for future research in this domain.

The remainder of this paper is organized as follows. Section II reviews existing works on MLC, with a focus on noisy labels and SPML. Section III details the proposed method along with the theoretical analyses. The empirical evaluation is presented in Section IV, with the conclusion in Section V.

II. RELATED WORKS

This section reviews advancements in MLC, with emphasis on RS applications, challenges from noisy labels, and recent SPML methods developed in CV.

A. Remote Sensing Image Multi-label Classification

Early DL research in MLC for RS imagery primarily focused on high-resolution data and employed Convolutional Neural Networks (CNNs) for feature extraction, followed by classifiers such as Radial Basis Function Neural Networks [20] or Structured Support Vector Machines [21]. These approaches often relied on conventional transfer learning, using CNNs pre-trained on generic CV datasets (e.g., ImageNet [22]) as fixed feature extractors. However, the significant differences between natural CV scenes and complex RS imagery can lead to suboptimal classification performance, limiting the effectiveness of such direct transfer.

To mitigate the limitations of pre-trained models, alternative strategies have been proposed. For instance, Stivaktakis *et al.* [23] introduced a data augmentation scheme to facilitate end-to-end training of shallow CNNs, along with replacing the softmax layer with a sigmoid function to accommodate multi-label outputs. While this direct adaptation remains a common practice in multi-label scenarios, it may result in the imprecise identification of multiple classes. More sophisticated approaches integrate sequential neural network architectures with CNNs to enhance multi-label scene classification. Hua *et al.* [6] proposed a class-wise attention-based Recurrent Neural Network (RNN) to explicitly model the co-occurrence relationships among multiple classes, thus generating class predictions sequentially. Similarly, an attention-aware label relational reasoning network was introduced in [11] to localize discriminative regions and characterize inter-label relationships based on feature maps. Alshehri *et al.* [24] presented an encoder-decoder neural network architecture, where the encoder includes a squeeze-and-excitation layer to model channel-wise dependencies, and the RNN-based decoder serves as an adaptive spatial attention module. These attention-driven strategies have demonstrated considerable success in identifying informative areas through attention maps derived from convolutional features.

B. Multi-label Classification with Noisy Labels

A major hurdle in MLC in RS is the difficulty in obtaining exhaustive multi-label annotations, which often results in noisy labels. This noise can be categorized as either missing labels (subtractive noise), where a class present in the considered image is not annotated, or as wrong labels (additive noise),

where an absent class is incorrectly annotated [8]. Such multi-label noise, which can be introduced through zero-cost annotation (*e.g.*, using thematic products), can severely impair model training. Consequently, developing methods robust to multi-label noise in RS is an active research area, usually categorized as weakly supervised multi-label learning (WSML) [25].

Methods for handling noisy labels in multi-label settings often draw inspiration from related fields, such as positive-unlabeled learning (PUL) [26]–[28] and noisy multi-class learning [29]. Common strategies involve developing robust loss functions that are less sensitive to label noise or class imbalance [30]. Another approach is pseudo-labeling, where likely labels for unobserved or unknown annotations are inferred to provide additional training signals [31]. The “memorization effect,” where models tend to learn clean labels early but later start to memorize noisy ones, has been widely observed in noisy MCC. Early Learning Regularization (ELR) [32] was developed to specifically counteract this, by adjusting the influence of gradients from potentially noisy samples, particularly in the early stages of training. Burgert *et al.* [8] later extended it to MLC in a straightforward manner and empirically demonstrated its effectiveness. Additional strategies include sample selection, which aims to identify and potentially exclude noisy labels [33], label correction/refurbishment, which attempts to correct noisy labels (*e.g.*, using collaborative learning frameworks [34], [35]), and noise-robust regularization, such as using word embedding similarities to regularize model training [36].

Other methods, such as those in the large loss (LL) [14] family, including LL-R, LL-Ct, and LL-Cp, are developed to recognize and handle mislabeled samples with large losses, based on the observation that noisy labels often lead to high loss values. Specifically, LL-R rejects samples with large losses, LL-Ct applies temporary corrections, and LL-Cp employs permanent corrections. BoostLU [17] complements LL by enhancing predicted positive regions via a function applied to class activation maps (CAMs), further improving the robustness.

In WSML for RS, subtractive noise, *i.e.*, missing true labels, is a prevalent issue. This often occurs because annotators, especially when facing complex imagery or large datasets, opt to label only the dominant class(es) rather than exhaustively identify all present categories. This poses a significant challenge because an unannotated class doesn't necessarily mean its absence, leading to the extreme case of subtractive noise known as SPML. This scenario is both challenging and increasingly common in practical RS applications, despite being underexplored in the RS literature.

C. Single Positive Multi-Label Learning

SPML was formally defined by Cole *et al.* [10] as the scenario where each training image is annotated with only one positive label, while all other labels remain unobserved. A naive approach, such as Ignoring Unobserved (IU) labels, is insufficient in SPML and typically results in the model collapsing to predicting all labels as positive because of the complete lack of negative constraints. Therefore, the most common

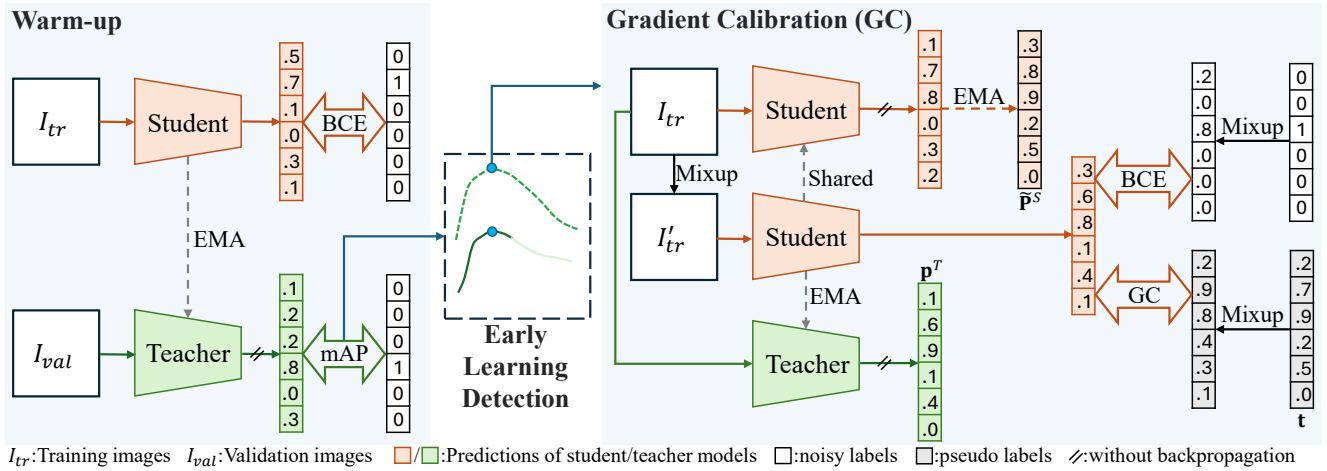
baseline in SPML is the AN loss, which treats all unobserved labels as negative during training. While straightforward, this assumption inherently introduces false negative labels, which can negatively impact model performance and generalization. To mitigate these challenges, Cole *et al.* [10] proposed several modified baseline methods for MLC. For instance, AN with label smoothing (AN-LS) applies label smoothing to reduce the penalty associated with potentially incorrect negative labels. Weak AN (WAN) introduces a weighting mechanism to down-weight the contribution of assumed negative labels in the loss computation. Other methods focus on regularizing model predictions or inferring missing labels. Expected Positives Regularization (EPR) is a regularization technique for IU that constrains the expected number of positive labels per image, helping in preventing the trivial solution of predicting all labels as positive. Building upon this, Regularized Online Label Estimation (ROLE) [10] treats unannotated labels as learnable parameters, estimated online during training and regularized with EPR.

Pseudo-labeling is another widely adopted strategy in SPML. In this case, a Label-Aware Global Consistency (LAGC) [15] regularization term is introduced to recover pseudo-labels, leveraging the data manifold structure learned through contrastive learning and data augmentation. Generalized Robust Loss (GR Loss) [16] provides a unified approach to SPML that incorporates soft pseudo-labels into a robust loss design to handle false negatives and class imbalance. Mutual label enhancement for sIngle-positive Multi-label LEarning (MIME) [18], based on the Variational Information Bottleneck (VIB) concept [37], is an iterative method that generates and refines pseudo-labels by maximizing the mutual information between model predictions and estimated pseudo-labels. Methods from PUL are also relevant, which focus on the single binary classification counterpart of SPML. The basic idea is to exploit an unbiased estimator of the empirical risk, which is only possible with the knowledge of the prior distribution of the positive class. For example, Dist-PU [38] exploits the positive class prior, along with Mixup [13], to address negative prediction bias and encourage confident predictions. While designed for PUL, it can be easily employed in SPML by independently applying it to each class.

However, the above-mentioned methods are mainly developed for natural images, and their direct application to RS data often falls short due to the distinct characteristics of RS imagery. Moreover, while pseudo-labeling has shown effective, it typically requires a warm-up stage to ensure label quality. Manually determining this stage can be suboptimal, either due to insufficient learning or overfitting to noisy labels.

III. METHODOLOGY

As illustrated in Fig. 2, the proposed method adopts a student-teacher architecture, where the teacher model's weights are updated via EMA. The training pipeline consists of two stages. In the first stage, the student model is trained directly on noisy labels, during which the teacher model's validation accuracy (with respect to noisy labels) is monitored as an early learning indicator to determine when to activate the second



stage—Gradient Calibration (GC). Next, we first define the problem before presenting the technical details of AdaGC.

A. Problem Definition

In SPML, each image $\mathbf{x}_i \in \mathbb{R}^{h \times w \times d}$ is associated with a true label vector $\mathbf{y}_i^* \in \{0, 1\}^C$, where multiple labels may be relevant. However, during training, only a single positive label is observed per image. The observed label vector $\mathbf{y}_i \in \{0, 1\}^C$ satisfies the following conditions:

$$\mathbf{y}_i \preceq \mathbf{y}_i^*, \quad \|\mathbf{y}_i\|_1 = 1, \quad (1)$$

where C is the total number of classes and \preceq denotes element-wise no-larger-than comparison. Specifically, for two binary vectors $\mathbf{a}, \mathbf{b} \in \{0, 1\}^C$, $\mathbf{a} \preceq \mathbf{b}$ if $a_j \leq b_j, \forall j$.

The objective is to train a multi-label classifier f parametrized by weights θ to recover the complete set of labels despite incomplete supervision. The common AN strategy treats all unobserved labels as negatives. This leads to the standard binary cross-entropy (BCE) loss:

$$\mathcal{L}_{\text{AN}}(\theta) = - \sum_{i=1}^N \sum_{c=1}^C [y_{i,c} \log p_{i,c} + (1 - y_{i,c}) \log (1 - p_{i,c})], \quad (2)$$

where $\mathbf{p}_i = \text{Sigmoid}(f(\mathbf{x}_i; \theta)) \in [0, 1]^C$. However, this approach can easily lead to overfitting to label noise by incorrectly penalizing potentially relevant but unobserved labels.

B. Gradient Calibration

The concept of gradient calibration for handling noisy labels was first proposed in [32] for MCC, where ELR introduces an auxiliary regularization term to constrain the standard cross-entropy loss, thus preventing the memorization of noisy labels. The regularization term for MCC is defined as follows:

$$\mathcal{R}_{\text{MCC}}(\theta) = \frac{1}{n} \sum_{i=1}^n \log (1 - \langle \mathbf{p}_i, \mathbf{t}_i \rangle). \quad (3)$$

Here, both \mathbf{p}_i and \mathbf{t}_i are probability vectors whose elements are non-negative and sum to 1. This simplex constraint ensures

that their inner product $\langle \mathbf{p}_i, \mathbf{t}_i \rangle$ lies within the range $[0, 1]$. The gradient of (3) is defined as follows:

$$\nabla_{\theta} \mathcal{R}_{\text{MCC}}(\theta) = \frac{1}{n} \sum_{i=1}^n \nabla_{\theta} f(\mathbf{x}_i; \theta) \cdot \mathbf{g}_i, \quad (4)$$

with $\mathbf{g}_i \in \mathbb{R}^C$, whose values are computed as follows:

$$g_{i,c} = \frac{p_{i,c}}{1 - \langle \mathbf{p}_i, \mathbf{t}_i \rangle} \sum_{k=1}^C (t_{i,k} - t_{i,c}) \cdot p_{i,k}. \quad (5)$$

As indicated by (5), the sign of (4) is governed by $t_{i,k} - t_{i,c}$. Specifically, the ELR regularization calibrates the gradients toward negative values when \mathbf{t}_i indicates that the class c is the potential correct label. Conversely, if class c is not favored by the pseudo label, the calibration term $g_{i,c}$ remains positive. This behavior is consistent with the gradient direction of the cross-entropy loss, which yields negative gradients for $y_{i,c} = 1$ and positive gradients for $y_{i,c} = 0$.

Equation (3) holds effective only for multi-class cases with $\|\mathbf{p}_i\|_1 = 1$ and $\|\mathbf{t}_i\|_1 = 1$. In the multi-label case, directly applying (3) leads to unbounded $\langle \mathbf{p}_i, \mathbf{t}_i \rangle$ that also varies significantly across samples due to differing numbers of positive labels. A straightforward adaptation is to extend it to a class-wise binary setting, that is,

$$\mathcal{R}_{\text{MLC}}^{\text{binary}}(\theta) = \frac{1}{n} \sum_{i=1}^n \sum_{c=1}^C \log (1 - \langle \mathbf{b}_{i,c}, \mathbf{t}_{i,c} \rangle), \quad (6)$$

where $\mathbf{b}_{i,c} = [p_{i,c}, 1 - p_{i,c}]^T$ is the binary prediction vector for sample i at class c , and $\mathbf{t}_{i,c} = [t_{i,c}, 1 - t_{i,c}]^T$. In general, negative labels ($y_{i,c} = 0$) vastly outnumber positive ones ($y_{i,c} = 1$) in multi-label datasets, even though each sample may be associated with multiple classes. Thus, (6) falls ineffective in practice, particularly in SPML settings, since the regularization term is largely dominated by calibration on $y_{i,c} = 0$, and overwhelms the contribution from the sparse positive labels.

To address this limitation, we emphasize the gradient calibration on the potential positive labels with the following regularization term:

$$\mathcal{R}_{\text{MLC}}^{\text{GC}}(\theta) = \frac{1}{n} \sum_{i=1}^n \sum_{c=1}^C \mathbb{I}(y_{i,c} = 0) \log(1 - p_{i,c} \cdot t_{i,c}), \quad (7)$$

where $\mathbb{I}(\text{True}) = 1$ otherwise 0. Considering the SPML setting, GC is applied only to negative labels, excluding its use for positive ones in practice. We can compute the gradient of (7) as follows:

$$\nabla_{\theta} \mathcal{R}_{\text{MLC}}^{\text{GC}}(\theta) = \frac{1}{n} \sum_{i=1}^n \sum_{c=1}^C \mathbb{I}(y_{i,c} = 0) \nabla_{\theta} f_c(\mathbf{x}_i; \theta) \cdot g_{i,c}, \quad (8)$$

where $g_{i,c}$ is defined as follows:

$$g_{i,c} = \frac{-t_{i,c}}{1 - p_{i,c} \cdot t_{i,c}} \cdot p_{i,c}(1 - p_{i,c}) \leq 0, \quad (9)$$

where $p_{i,c}(1 - p_{i,c})$ is the sigmoid derivative. We argue that (7) is particularly suitable for the SPML setting, as it specifically penalizes false negatives by pushing the model to predict positive scores for (negative) labels with higher pseudo-label scores $t_{i,c}$. The final objective is a combination of the binary cross-entropy loss and the GC regularization:

$$\mathcal{L}(\theta) = \mathcal{L}_{\text{AN}}(\theta) + \lambda \cdot \mathcal{R}_{\text{MLC}}^{\text{GC}}(\theta), \quad (10)$$

where λ is the weight of the regularization term.

However, applying GC from the beginning may lead the model to predict all classes as positive. Liu et al. [39] show that adaptively triggering correction before overfitting to label noise is crucial for the effectiveness of sample-correction-related techniques. Inspired by this, in Section III-C we introduce a simple early learning detection mechanism to appropriately activate GC. Moreover, as GC performance depends on the quality of the pseudo-labels \mathbf{t} , in Section III-D we design a dual-EMA module to ensure the robust generation of pseudo-labels.

C. Early Learning Detection

Pseudo-labelling methods typically require an initial warm-up phase to mitigate the trade-off between additive noise (premature initiation) and subtractive noise overfitting (excessive delay). Ideally, the optimal activation time is identified by the performance plateau on a clean validation set [39]–[41]. In SPML, where clean validation data is unavailable, we propose monitoring the mean average precision (mAP) on the noisy validation set. Below, we provide a formal justification for this criterion by analyzing the bounds and stationarity of the noisy metric.

1) *Theoretical Framework:* Let Rec_c^* and Prec_c^* denote the clean recall and precision for class c . In SPML, the set of real positives P_c is reduced by the flipped positives $F_c = \beta_c P_c$, where $\beta_c \in (0, 1)$ is the noise rate. Defining $\text{PF}_c = \alpha_c \cdot F_c$, where $\alpha_c \in [0, 1]$, as the proportion of correctly classified

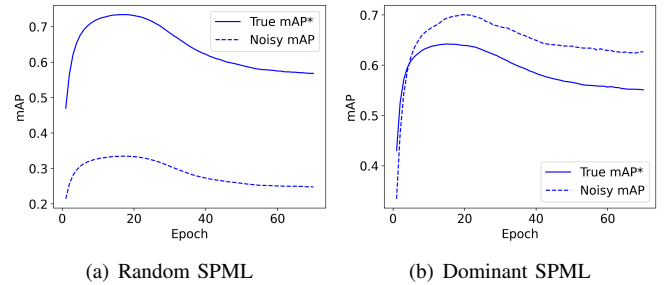


Fig. 3. True and noisy validation mAP trends of the teacher model during training on refined BigEarthNet [12]: (a) random SPML, (b) dominant SPML. The trends align with Propositions 1 and 2, and confirm the validity of the stationarity theorem.

flipped positives, the noisy metrics relate to the clean ones as follows:

$$\begin{aligned} \text{Rec}_c &= \frac{\text{TP}_c - \text{PF}_c}{\text{P}_c - \text{F}_c} = \frac{\text{Rec}_c^* - \alpha_c \beta_c}{1 - \beta_c}, \\ \text{Prec}_c &= \frac{\text{TP}_c - \text{PF}_c}{\text{PP}_c} = \text{Prec}_c^* \left(1 - \frac{\alpha_c \beta_c}{\text{Rec}_c^*}\right), \end{aligned} \quad (11)$$

where TP_c and PP_c are the true and predicted positives, respectively. The mAP is the macro average of average precision (AP) for each class:

$$\text{mAP} = \frac{1}{C} \sum_{c=1}^C \text{AP}_c, \quad (12)$$

where $\text{AP}_c = \int_0^1 \text{Prec}_c(\text{Rec}_c) d\text{Rec}_c$.

Proposition 1 (Random SPML Lower Bound). *Under instance-independent noise, the expected noisy mAP is a lower bound of the clean mAP*.*

Proof: In Random SPML, the noise is independent of the input features [42]. Thus, the model cannot generalize to the random flips, implying $\mathbb{E}[\alpha_c] \approx \text{Rec}_c^*$. Substituting this into (11) yields $\mathbb{E}[\text{AP}_c] \approx (1 - \beta_c)\text{AP}_c^*$. The expected noisy mAP becomes:

$$\mathbb{E}[\text{mAP}] \approx (1 - \bar{\beta})\text{mAP}^* - \text{Cov}(\beta, \text{AP}^*), \quad (13)$$

where $\bar{\beta}$ is the mean flip rate. Since better-performing classes generally experience less flipping (negative covariance), $\mathbb{E}[\text{mAP}] < \text{mAP}^*$. \square

Fig. 3(a) shows the trends observed while training on the refined BigEarthNet [12] dataset with random single-positive labels, which are aligned with our theoretical analysis.

Proposition 2 (Dominant SPML Upper Bound). *Under instance-dependent dominant noise, the expected noisy mAP is an upper bound of the clean mAP*.*

Proof: In Dominant SPML, the model learns the label-noise model [42], ignoring non-dominant true positives ($\mathbb{E}[\alpha_c] \rightarrow 0$). Eq. (11) simplifies to $\mathbb{E}[\text{Rec}_c] \approx \frac{\text{Rec}_c^*}{1 - \beta_c}$ and $\mathbb{E}[\text{Prec}_c] \approx \text{Prec}_c^*$, yielding $\mathbb{E}[\text{AP}_c] \approx \frac{1}{1 - \beta_c}\text{AP}_c^*$. The noisy mAP becomes:

$$\mathbb{E}[\text{mAP}] \approx \overline{\left(\frac{1}{1 - \beta}\right)}\text{mAP}^* + \text{Cov}\left(\frac{1}{1 - \beta}, \text{AP}^*\right). \quad (14)$$

Assuming dominant classes perform better (negative covariance), $\text{mAP}^* < \mathbb{E}[\text{mAP}]$. \square

Generally, Dominant SPML results in three consecutive trends during learning [39]: i) an early learning phase where $\mathbb{E}[\alpha_c] \approx \text{Rec}_c^*$ still holds, yielding similar results to random SPML; ii) a transition phase; and iii) a label-noise model fitting phase. Fig. 3(b) plots the trends observed while training on the refined BigEarthNet [12] dataset with dominant single-positive labels, showing this three-phase phenomenon.

2) *Adaptive Triggering Mechanism*: We now address the validity of using the noisy metric for early stopping.

Theorem 1 (Stationarity Preservation). *The stationary points of the expected noisy mAP coincide with those of the clean mAP* in the late early-learning phase.*

Proof: Let t denote the training epoch. Combining Propositions 1 and 2, the noisy metric is a linear transformation of the clean metric: $\mathbb{E}[\text{mAP}(t)] = \bar{\omega}\text{mAP}^*(t) + \text{Cov}(\omega, \text{AP}^*(t))$. Taking the temporal derivative:

$$\frac{\partial \mathbb{E}[\text{mAP}]}{\partial t} = \bar{\omega} \frac{\partial \text{mAP}^*}{\partial t} + \frac{\partial}{\partial t} \text{Cov}(\omega, \text{AP}^*(t)). \quad (15)$$

The noise parameters ω are constant. Near the performance plateau ($t \rightarrow t^*$), class-wise learning dynamics tend to stabilize, making the covariance term approximately constant at that time ($\frac{\partial}{\partial t} \text{Cov} \approx 0$). Consequently:

$$\frac{\partial \mathbb{E}[\text{mAP}]}{\partial t} \propto \frac{\partial \text{mAP}^*}{\partial t}. \quad (16)$$

Thus, identifying the peak of the noisy mAP is mathematically equivalent to identifying the peak of the clean mAP. \square

Implementation: To mitigate stochastic fluctuations in the single-run estimates of $\mathbb{E}[\text{mAP}]$, we monitor the mAP of the teacher model (maintained via EMA), which acts as a low-pass filter on the model's weights (see Fig. 6). We select the epoch maximizing the teacher's noisy validation mAP (with a patience of b_e epochs) to initiate pseudo-labeling.

D. Dual-EMA Pseudo-Label Generation

As discussed in Section III-B, GC relies on high-quality pseudo-labels. The teacher's predictions are a natural choice, since the early learning detection is on the teacher model. However, due to slow weight updates, the teacher model may exhibit a delay in incorporating recently acquired knowledge after GC begins. Therefore, we propose to combine predictions from both teacher and student models. Specifically, we apply EMA to the student's predictions with a smaller smoothing factor than that for the teacher model, to avoid overfitting to its own outputs while maintaining adaptability.

Let \mathbf{p}_i^T and \mathbf{p}_i^S denote the prediction probabilities of the teacher and student models for sample i , respectively. For the teacher model, we have the following:

$$\mathbf{p}_i^T(e) = f(\mathbf{x}_i; \theta^T(e)), \quad (17)$$

$$\theta^T(e) = \beta_t \cdot \theta^T(e-1) + (1 - \beta_t) \cdot \theta^S(e) \quad (18)$$

with $\theta^T(e)$ and $\theta^S(e)$ being the model weights of the teacher and student models at iteration e . We set the smoothing coefficient $\beta_t = 0.999$ following [43]. Then, the temporally EMA-smoothed student predictions are as follows:

$$\tilde{\mathbf{p}}_i^S(e) = \beta_s \cdot \tilde{\mathbf{p}}_i^S(e-1) + (1 - \beta_s) \cdot \mathbf{p}_i^S(e). \quad (19)$$

We empirically set $\beta_s = 0.8$ to guarantee the update speed of the student's predictions. Then, the pseudo-label $\mathbf{t}_i(e)$ used for gradient calibration is computed as the combination of the teacher and student predictions as follows:

$$\mathbf{t}_i = \gamma \cdot \mathbf{p}_i^T + (1 - \gamma) \cdot \tilde{\mathbf{p}}_i^S, \quad (20)$$

where e is omitted for simplicity. In our experiments, we set $\gamma = 0.5$ to balance the contributions of the teacher and student models when generating pseudo-labels.

E. Mixup

To further enhance robustness against label noise and improve generalization, we incorporate Mixup [13] into the GC stage. For each batch, we randomly sample a pairing input $(\mathbf{x}_j, \mathbf{y}_j, \mathbf{t}_j)$ for every original input $(\mathbf{x}_i, \mathbf{y}_i, \mathbf{t}_i)$, and compute:

$$\tilde{\mathbf{z}}_i = \phi \cdot \mathbf{z}_i + (1 - \phi) \cdot \mathbf{z}_j \quad \text{for } \mathbf{z} \in \{\mathbf{x}, \mathbf{y}, \mathbf{t}\}, \quad (21)$$

where $\phi \sim \text{Beta}(\alpha, \alpha)$ and $\alpha > 0$ controls the interpolation strength. The mixed samples $(\tilde{\mathbf{x}}_i, \tilde{\mathbf{y}}_i, \tilde{\mathbf{t}}_i)$ are then used for training during the GC phase. This data augmentation encourages linear behavior between examples, mitigates overfitting, and stabilizes training under noisy labels.

F. Complexity Analysis

To assess practical feasibility, we analyze the computational complexity of AdaGC relative to a standard classification baseline. First, one can note that AdaGC is a training-only framework, *i.e.*, the dual-EMA module is discarded after training. Consequently, the inference complexity (parameters and FLOPs) is identical to the student backbone, ensuring no additional latency or memory overhead during deployment.

Regarding training efficiency, a standard iteration incurs a cost of approximately $3 \times$ the forward pass FLOPs (1F forward and ~ 2 F backward). Instead, AdaGC processes two views during the GC stage: the original batch and a Mixup-augmented batch. However, the original batch is utilized exclusively for generating robust pseudo-labels via the student and teacher networks, which requires only forward passes, while the model optimization relies on the Mixup batch. Therefore, the computationally intensive backward pass is strictly necessary only for this view. This design results in a total theoretical cost of ~ 5 F per iteration, representing a moderate $\sim 66\%$ overhead compared to the baseline (3F) exclusively during the GC stage. Note that Mixup is simply a linear combination of two images. Thus, its additional FLOPs are mathematically negligible compared to the rest of the pipeline.

In terms of memory complexity, the overhead is modest. The teacher EMA maintains only a second copy of the backbone parameters (not activations), contributing less than 10% of total memory in typical large-scale models. The temporally smoothed student predictions are stored as image-wise labels, which also require minimal memory. Taken together, both FLOPs and memory considerations indicate that AdaGC is computationally feasible for large-scale remote sensing applications.

TABLE I

REFINED BIGEARTHNET LAND COVER CLASSES AND RELATED FLIP RATES β_c ON THE TRAINING SUBSET IN THE TWO CASES OF RANDOM AND DOMINANT SPML LABEL NOISE

Class Name	Random β_c	Dominant β_c	Support
Urban fabric	0.73	0.84	33,626
Industrial or commercial units	0.72	0.91	6,398
Arable land	0.63	0.51	88,236
Permanent crops	0.70	0.74	15,190
Pastures	0.66	0.62	42,968
Complex cultivation patterns	0.73	0.77	51,034
Land principally occupied by agriculture, with significant areas of natural vegetation	0.73	0.86	60,127
Agro-forestry areas	0.64	0.54	15,082
Broad-leaved forest	0.69	0.65	64,164
Coniferous forest	0.66	0.54	76,344
Mixed forest	0.70	0.67	78,791
Natural grassland and sparsely vegetated areas	0.69	0.82	6,984
Moors, heathland and sclerophyllous vegetation	0.70	0.70	6,329
Transitional woodland, shrub	0.70	0.85	64,198
Beaches, dunes, sands	0.72	0.94	738
Inland wetlands	0.67	0.78	11,344
Coastal wetlands	0.70	0.70	670
Inland waters	0.67	0.73	30,466
Marine waters	0.08	0.05	35,914
Micro average	0.65	0.65	—
Macro average $\bar{\beta}$	0.66	0.70	—
Average number of true positive labels per image		2.9	

IV. EXPERIMENTS

This section presents the experimental setups, comparative results, and a comprehensive ablation study of AdaGC.

A. Datasets

We evaluate the proposed method on two multi-label RS benchmark datasets with different modalities and resolutions: refined BigEarthNet (reBEN) [12], [44], [45], derived from SAR and multispectral Sentinel-1/2 imagery at 10m resolution, and AID-multilabel [11], derived from high-resolution RGB images at 0.5–8m resolution. While reBEN focuses on land cover classification, AID-multilabel includes both land cover categories and object-level semantic information.

1) *reBEN*: It contains 549,488 Sentinel-1/2 image pairs of size of 120×120 pixels covering 10 European countries, each aligned with a pixel-level CORINE Land Cover (CLC) reference map. Multi-label annotations are derived from these maps, resulting in 19 land cover classes (see Table I). Following the splits in [12], we use a 2:1:1 ratio for training, validation, and testing. Each input has 14 channels by concatenating 2 Sentinel-1 and 12 Sentinel-2 L2A bands. Leveraging the reference maps, on this dataset we simulate both types of SPML label noise described in Section III-C (*Random* and *Dominant*). The *Dominant* case better reflects real-world

TABLE II

AID MULTILABEL CLASSES AND RELATED FLIP RATES β_c ON THE TRAINING SUBSET IN THE TWO CASES OF RANDOM AND MANUAL SPML LABEL NOISE

Class Name	Random β_c	Manual β_c	Support
Airplane	0.83	0.80	59
Bare-soil	0.80	0.78	882
Buildings	0.82	0.81	1,316
Cars	0.85	0.85	1,210
Chaparral	0.76	0.85	79
Court	0.86	0.78	203
Dock	0.94	0.83	166
Field	0.66	0.57	127
Grass	0.78	0.80	1,368
Pavement	0.83	0.84	1,367
Sand	0.41	0.48	153
Sea	0.77	0.67	133
Ship	0.90	0.89	181
Tanks	0.82	0.73	66
Trees	0.79	0.80	1,467
Water	0.83	0.84	510
Micro average	0.81	0.81	—
Macro average $\bar{\beta}$	0.79	0.77	—
Average number of true positive labels per image		5.2	

single-positive annotations, as low-resolution images contain limited details, where the prevailing class is more likely to be observed while minor classes are ignored. Dataset statistics for the two cases are provided in Table I.

2) *AID-multilabel*: It extends the AID scene classification dataset [46] with multi-label annotations. The dataset comprises 3,000 high-resolution RGB aerial image patches (600×600 pixels) across 17 classes, collected from China, U.S., and several European countries. We exclude the extremely rare “mobile home” class (only 2 samples), resulting in 16 classes. Following [11], 20% of the data is held out for testing. We then use 25% of the remaining training set for validation. Unlike reBEN, AID’s high spatial resolution allows multiple objects to be easily recognized, making it difficult to identify a single dominant class. Therefore, in addition to *Random* simulation, we manually annotated the AID dataset in a single-positive manner to assess model performance under realistic SPML conditions. For each image, four randomly shuffled candidate classes were displayed at a time to speed up annotation, with the option to refresh if none were suitable. Consecutive images were also prevented from being assigned to the same class to reduce potential annotation bias. This procedure makes the *Manual* labels behave similarly to random SPML labels, yet retain a slight human selection bias. The entire annotation process took approximately 4.5 hours. We also found and corrected several label inconsistencies in the original AID-multilabel data, most of which are from the meadow folder. The corrected multi-label annotations, the manual single-positive labels, and the annotation tool will be released publicly along with the AdaGC code. Dataset statistics are provided in Table II. For simplicity,

TABLE III

TEST PERFORMANCE COMPARISON OF DIFFERENT METHODS ON THE reBEN-RANDOM DATASET. THE BEST AVERAGE METRIC VALUES ARE REPORTED IN BOLD, SECOND BESTS ARE IN ITALIC. THE RELATED STANDARD DEVIATIONS ARE REPORTED IN BRACKETS

		mAP (%) ↑	Coverage ↓	Rankloss (%) ↓	OA (%) ↑	mF1 (%) ↑	mprecision (%) ↑	mrecall (%) ↑
Ground-truth Training	GT w/ BCE	71.75 (0.04)	4.264 (0.003)	3.428 (0.005)	93.09 (0.01)	66.63 (0.12)	72.07 (0.02)	63.24 (0.35)
	IUN	70.46 (0.11)	4.331 (0.009)	3.608 (0.024)	91.98 (0.01)	56.00 (0.19)	84.75 (0.55)	44.66 (0.18)
Baseline Methods	AN	54.97 (0.12)	4.849 (0.002)	5.847 (0.003)	87.13 (0.04)	28.15 (0.30)	72.93 (1.67)	19.00 (0.21)
	AN-LS	54.40 (0.66)	5.375 (0.114)	7.051 (0.309)	86.90 (0.03)	25.47 (0.44)	75.90 (0.73)	17.07 (0.31)
	WAN	59.43 (0.34)	4.660 (0.010)	5.089 (0.037)	90.16 (0.05)	60.15 (0.20)	55.96 (0.36)	66.14 (0.65)
	EPR ^a	50.74 (0.40)	5.206 (0.022)	6.825 (0.053)	80.13 (0.08)	51.22 (0.11)	38.25 (0.13)	85.59 (0.19)
General Label Noise Methods	ELR	62.40 (0.08)	4.860 (0.021)	4.890 (0.021)	91.45 (0.04)	63.97 (0.07)	62.63 (0.36)	68.26 (0.25)
	LL-Cp	57.27 (0.13)	4.983 (0.013)	6.068 (0.038)	89.60 (0.03)	49.35 (0.58)	65.47 (0.40)	43.67 (0.88)
	LL-Ct	62.35 (0.23)	4.722 (0.010)	4.856 (0.029)	91.76 (0.03)	54.87 (0.35)	76.27 (1.09)	46.41 (0.18)
	LL-R	59.70 (0.27)	4.688 (0.012)	5.054 (0.042)	90.85 (0.05)	53.91 (0.56)	70.44 (1.08)	45.45 (0.45)
PUL Methods	BoostLU	61.77 (0.63)	4.662 (0.011)	4.780 (0.023)	91.59 (0.01)	55.41 (0.61)	74.80 (1.30)	46.32 (0.36)
	Dist-PU ^a	61.98 (0.26)	4.860 (0.016)	5.111 (0.024)	90.67 (0.04)	61.49 (0.35)	59.11 (0.47)	68.83 (0.52)
SPML Methods	ROLE	55.73 (0.36)	6.479 (0.007)	6.424 (0.020)	91.18 (0.05)	59.65 (0.31)	61.90 (0.45)	58.36 (0.35)
	GR	57.38 (0.49)	4.914 (0.034)	5.855 (0.120)	89.77 (0.08)	56.79 (0.85)	57.91 (0.16)	56.06 (1.56)
	LAC	57.88 (0.30)	4.801 (0.021)	5.384 (0.036)	87.33 (0.25)	28.97 (1.38)	72.29 (0.62)	19.85 (1.11)
	MIME	58.64 (0.35)	4.894 (0.017)	5.632 (0.064)	90.66 (0.13)	55.13 (0.36)	62.40 (0.46)	50.39 (0.21)
RS-specific Methods	RCML	64.91 (0.12)	4.585 (0.005)	4.467 (0.020)	91.24 (0.04)	52.90 (0.32)	78.57 (1.29)	42.42 (0.34)
	LCR	54.56 (0.32)	4.864 (0.009)	5.912 (0.044)	87.16 (0.03)	28.52 (0.14)	73.82 (1.81)	19.31 (0.08)
Proposed	AdaGC	67.85 (0.05)	4.553 (0.012)	4.165 (0.033)	92.49 (0.01)	64.46 (0.24)	70.43 (0.59)	63.22 (0.10)

^a EPR and Dist-PU use additional a-priori information, which is assumed unknown in all other approaches.

in the following we use AID to refer to AID-multilabel.

B. Experimental Setup

We adopt ResNet-34 and ResNet-50 as backbones for the reBEN and AID datasets, with batch sizes of 512 and 32, respectively. ResNet-34 is chosen for reBEN as an efficient compromise, since our focus is on evaluating method effectiveness rather than maximizing absolute accuracy. For AID, we use ImageNet-pretrained weights given its RGB input. To adhere to a realistic weakly supervised scenario where ground-truth multi-labels are unavailable, we strictly avoid the use of clean data for model selection. Consequently, all hyperparameters are tuned via grid search on the noisy validation set, simulating the absence of clean labels. While this strategy relies on imperfect supervision, it prevents the introduction of “oracle” information and ensures that the reported performance reflects the method’s capability to generalize without privileged access to clean labels. Despite the use of noisy validation labels, the resulting metrics remain informative for model selection. Under SPML noise, random errors are inherently difficult for deep models to memorize, and thus the validation signal largely reflects the underlying clean structure. As confirmed in our experiments, noisy mAP validation scores maintain a strong correlation with clean test performance, making them a practical and reliable indicator in the absence of ground-truth labels. To reduce computational cost, tuning is performed on subsets (20% for reBEN, 50% for AID) and fewer epochs (10) for comparison methods. For AdaGC, the Mixup Beta parameter α is set to 1. The GC loss weight λ is set to 3, 5, 9, and 8 for reBEN-*Random*, reBEN-*Dominant*, AID-*Random* and AID-*Manual*, respectively, and the learning rate is set to

1e-3 and 5e-4 for reBEN and AID, respectively, based on tuning results.

For the final evaluation, all models are trained for 70 epochs on the full training sets using the optimal hyperparameters and evaluated on the clean test sets. To ensure robustness and statistical reliability, each experiment is repeated for three Monte Carlo runs. We report the mean and unbiased standard deviation of all metrics.

In addition to mAP, we report two ranking-based metrics, *i.e.*, coverage and ranking loss (Rankloss), and four accuracy-based metrics, *i.e.*, overall accuracy (OA), mean F1 score (mF1), mean precision (mprecision), and mean recall (mrecall). The metrics are defined as follows.

- **Coverage** measures how far we need to go down the ranked label list to cover all true labels:

$$\frac{1}{N} \sum_{i=1}^N \max_{y \in \mathbf{y}_i} \text{rank}_f(\mathbf{x}_i, y) - 1, \quad (22)$$

where $\text{rank}_f(\mathbf{x}_i, y)$ is the position of the ground-truth (GT) label $y_{i,c}$ in the ranking list predicted by f ;

- **Ranking loss** computes the average fraction of label pairs that are incorrectly ordered:

$$\frac{1}{N} \sum_{i=1}^N \frac{1}{|\mathbf{y}_i| |\overline{\mathbf{y}}_i|} \sum_{(y_1, y_0) \in \mathbf{y}_i \times \overline{\mathbf{y}}_i} \mathbb{I}(f(\mathbf{x}_i, y_1) \leq f(\mathbf{x}_i, y_0)), \quad (23)$$

where \mathbf{y}_i and $\overline{\mathbf{y}}_i$ are the sets of relevant (positive) and irrelevant (negative) labels, respectively, and $\mathbb{I}(\text{True}) = 1$ otherwise 0;

TABLE IV

TEST PERFORMANCE COMPARISON OF DIFFERENT METHODS ON THE REBEN-DOMINANT DATASET. THE BEST AVERAGE METRIC VALUES ARE REPORTED IN **BOLD**, SECOND BESTS ARE IN **ITALIC**. THE RELATED STANDARD DEVIATIONS ARE REPORTED IN BRACKETS

		mAP (%) ↑	Coverage ↓	Rankloss (%) ↓	OA (%) ↑	mF1 (%) ↑	mprecision (%) ↑	mrecall (%) ↑
Ground-truth Training	GT w/ BCE	71.75 (0.04)	4.264 (0.003)	3.428 (0.005)	93.09 (0.01)	66.63 (0.12)	72.07 (0.02)	63.24 (0.35)
	IUN	64.46 (0.07)	5.289 (0.013)	5.908 (0.007)	90.78 (0.01)	47.38 (0.09)	86.11 (0.95)	35.73 (0.06)
Baseline Methods	AN	55.91 (0.29)	6.533 (0.075)	8.128 (0.084)	88.70 (0.01)	34.25 (0.26)	84.35 (0.49)	24.08 (0.15)
	AN-LS	53.65 (0.12)	8.474 (0.088)	14.878 (0.282)	88.61 (0.00)	33.93 (0.16)	85.99 (0.99)	23.75 (0.12)
	WAN	58.69 (0.28)	6.627 (0.054)	8.153 (0.044)	90.76 (0.02)	50.56 (0.27)	74.22 (1.12)	41.50 (0.14)
	EPR ^a	49.15 (0.36)	6.150 (0.034)	9.003 (0.107)	87.22 (0.07)	53.34 (0.20)	48.48 (0.47)	64.38 (0.39)
General Label Noise Methods	ELR	54.48 (0.33)	9.149 (0.015)	11.429 (0.087)	91.02 (0.02)	50.08 (0.10)	76.38 (0.81)	42.05 (0.13)
	LL-Cp	47.70 (0.20)	6.061 (0.016)	8.968 (0.012)	88.04 (0.04)	53.17 (0.11)	51.47 (0.49)	59.48 (0.30)
	LL-Ct	54.11 (0.27)	6.287 (0.107)	8.014 (0.216)	90.88 (0.14)	53.67 (0.12)	70.67 (0.90)	47.82 (0.25)
	LL-R	54.41 (0.13)	7.369 (0.081)	8.662 (0.055)	91.01 (0.02)	53.59 (0.20)	70.83 (0.96)	46.88 (0.16)
PUL Methods	BoostLU	47.36 (0.34)	6.711 (0.110)	9.767 (0.376)	88.62 (0.21)	54.70 (0.45)	57.40 (1.38)	58.96 (0.46)
	Dist-PU ^a	53.51 (0.32)	6.224 (0.109)	8.770 (0.260)	88.23 (0.09)	53.17 (0.29)	56.21 (1.78)	60.53 (0.17)
	ROLE	48.54 (0.41)	12.465 (0.083)	14.591 (0.157)	90.81 (0.03)	50.24 (0.46)	75.38 (1.05)	40.88 (0.47)
SPML Methods	GR	55.73 (0.23)	5.765 (0.050)	7.238 (0.097)	89.20 (0.00)	38.28 (0.18)	81.43 (0.56)	27.57 (0.16)
	LAC	54.67 (0.56)	6.029 (0.074)	8.170 (0.206)	88.57 (0.02)	33.43 (0.63)	80.57 (1.58)	23.67 (0.37)
	MIME	55.61 (0.07)	6.417 (0.061)	8.982 (0.125)	89.90 (0.03)	43.54 (0.39)	76.38 (1.19)	33.36 (0.55)
RS-specific Methods	RCML	58.26 (0.82)	5.890 (0.134)	8.035 (1.181)	88.73 (1.05)	40.75 (1.27)	83.06 (2.35)	30.93 (2.88)
	LCR	55.64 (0.20)	6.579 (0.045)	8.151 (0.080)	88.67 (0.00)	34.25 (0.06)	83.24 (0.54)	24.05 (0.04)
Proposed	AdaGC	60.06 (0.16)	5.581 (0.026)	6.877 (0.054)	90.00 (0.06)	59.08 (0.25)	60.19 (0.47)	63.43 (0.37)

^a EPR and Dist-PU use additional a-priori information, which is assumed unknown in all other approaches.

- **OA** measures the percentage of samples with all labels correctly predicted:

$$\frac{1}{N} \sum_{i=1}^N \sum_{c=1}^C \mathbb{I}(\hat{\mathbf{y}}_{i,c} = \mathbf{y}_{i,c}); \quad (24)$$

- **mF1** is the average of F1-scores computed per class:

$$\frac{1}{C} \sum_{c=1}^C \frac{2 \cdot \text{Prec}_c \cdot \text{Rec}_c}{\text{Prec}_c + \text{Rec}_c}. \quad (25)$$

We compared AdaGC against a wide array of existing methods, categorized as follows.

- **Baseline methods:** We considered several baselines [10], such as AN, AN-LS, WAN, and EPR. All use a BCE loss at their core, while EPR uses only the BCE positive term and adds a regularization term, assuming the a-priori knowledge of the average number of positive labels per sample (see Tables I and II).
- **General label noise methods:** From this category, we considered the ELR approach adapted as in [8], the LL family of approaches (*i.e.*, LL-R, LL-Ct, and LL-Cp) [14], and the BoostLU [17] in combination with LL-Ct.
- **PUL methods:** We considered a single state-of-the-art (SOTA) method from this category, *i.e.*, Dist-PU [38], adapted for SPML by simply applying it to each class independently.
- **SPML-specific methods:** The main comparison methods we considered for SPML are ROLE [10], GR Loss [16], LAGC [15], and MIME [18].
- **Upper bound methods:** For analytical comparison with GT training, we considered two cases: i) training with GT multi-labels using a BCE loss (GT w/ BCE), and ii)

the IU with true Negatives (IUN) approach [10], where in addition to the single positive labels, all true negatives are provided for training. IUN allows us to assess the performance in a hypothetical scenario where all true negatives have been retrieved. False negatives are ignored during training, meaning that the model is still provided with a single positive label for each image.

• **RS-specific methods:** We also included RCML [35] and LCR [36], which were originally developed for general noisy multi-label RS classification. RCML leverages a collaborative learning framework with a ranking loss for sample selection to mitigate label noise, while LCR uses word embedding similarity to regularize model training under noisy annotations. To adapt them to SPML, we use only the missing-class labels term in RCML and perform selection per class rather than per sample. For LCR, we use RemoteCLIP's [47] text encoder to encode multi-word class names. These adaptations ensure a fair comparison while preserving the core noise-robust strategies of the original methods.

C. Benchmark Results

This section analyzes the benchmark results reported in Tables III–VI. Across all scenarios, AdaGC consistently achieves the highest mAP and strong SPML performance in terms of coverage, rankloss, and mF1, demonstrating its effectiveness and robustness in handling SPML in RS imagery. The upper-bound IUN performs well in mAP but suffers from low mrecall due to its inherent single-positive bias. AN and AN-LS are highly sensitive to false negatives, exhibiting high mprecision but low mrecall and consequently poor mAP. In contrast, WAN

TABLE V

TEST PERFORMANCE COMPARISON OF DIFFERENT METHODS ON THE AID-RANDOM DATASET. THE BEST AVERAGE METRIC VALUES ARE REPORTED IN BOLD, SECOND BESTS ARE IN ITALIC. THE RELATED STANDARD DEVIATIONS ARE REPORTED IN BRACKETS

		mAP (%) ↑	Coverage ↓	Rankloss (%) ↓	OA (%) ↑	mF1 (%) ↑	mprecision (%) ↑	mrecall (%) ↑
Ground-truth Training	GT w/ BCE	89.01 (0.32)	5.834 (0.011)	1.657 (0.061)	94.29 (0.19)	83.12 (0.66)	88.87 (0.38)	79.58 (1.28)
	IUN	82.24 (0.61)	6.622 (0.031)	3.408 (0.026)	90.88 (0.19)	72.65 (0.33)	93.13 (0.86)	62.87 (0.49)
Baseline Methods	AN	64.89 (1.28)	8.557 (0.164)	11.360 (0.351)	71.60 (0.23)	26.83 (0.18)	86.05 (2.18)	16.71 (0.13)
	AN-LS	64.40 (0.73)	11.347 (0.231)	21.664 (1.657)	70.65 (0.28)	19.97 (0.63)	79.98 (5.71)	12.14 (0.47)
	WAN	68.12 (0.46)	7.620 (0.173)	8.055 (0.588)	78.06 (0.16)	49.53 (0.42)	84.19 (1.05)	36.45 (0.27)
	EPR ^a	68.38 (1.84)	7.395 (0.079)	9.086 (0.412)	84.76 (0.57)	69.82 (1.10)	62.30 (0.85)	81.11 (1.68)
General Label Noise Methods	ELR	69.13 (0.73)	7.469 (0.063)	5.914 (0.152)	87.99 (0.12)	59.04 (0.84)	74.80 (1.00)	55.91 (0.30)
	LL-Cp	64.42 (1.06)	7.792 (0.141)	7.931 (0.471)	78.64 (0.58)	45.47 (1.25)	76.83 (3.94)	36.25 (0.78)
	LL-Ct	66.96 (1.60)	8.574 (0.243)	7.647 (0.322)	85.42 (0.65)	55.41 (0.91)	78.43 (4.80)	47.92 (0.75)
	LL-R	68.85 (0.44)	8.526 (0.018)	8.616 (0.294)	80.39 (0.58)	50.89 (2.19)	84.92 (2.85)	38.75 (2.31)
PUL Methods	BoostLU	68.00 (0.97)	8.104 (0.127)	6.656 (0.519)	85.44 (0.97)	54.48 (0.86)	79.19 (1.90)	47.14 (1.00)
	Dist-PU ^a	70.85 (0.47)	6.692 (0.133)	4.355 (0.265)	89.86 (0.09)	60.48 (3.26)	78.55 (6.93)	57.04 (3.10)
SPML Methods	ROLE	56.35 (0.77)	13.581 (0.041)	19.800 (0.282)	76.10 (0.38)	43.26 (0.73)	83.73 (3.32)	30.84 (0.57)
	GR	62.14 (0.73)	11.236 (0.090)	21.537 (0.567)	72.11 (0.09)	28.32 (0.56)	82.59 (4.41)	18.18 (0.32)
	LAC	62.27 (0.92)	7.902 (0.091)	9.674 (0.266)	72.57 (0.01)	28.59 (1.81)	82.17 (4.10)	18.38 (1.22)
	MIME	61.55 (1.86)	7.308 (0.175)	7.474 (0.756)	73.67 (0.26)	31.55 (1.32)	81.05 (3.42)	20.52 (0.86)
RS-specific Methods	RCML	64.24 (1.41)	7.522 (0.107)	8.338 (0.445)	80.10 (0.64)	45.45 (0.47)	75.62 (4.66)	37.84 (0.23)
	LCR	62.62 (0.47)	8.269 (0.165)	10.453 (0.500)	71.68 (0.13)	23.48 (1.01)	78.12 (2.50)	15.06 (0.58)
Proposed	AdaGC	75.67 (0.26)	6.862 (0.209)	5.636 (1.303)	83.39 (2.40)	64.16 (1.57)	68.89 (5.58)	71.82 (6.80)

^a EPR and Dist-PU use additional a-priori information, which is assumed unknown in all other approaches.

is more robust and achieves the best baseline mAP by better balancing precision-recall trade-offs. EPR, trained exclusively on positive labels with a cardinality regularizer, consistently shows the highest mrecall across datasets but low mprecision, reflecting its tendency to overestimate positives. Its advantage largely stems from the use of the true average number of labels per image, a prior not shared by other competitors. The two RS-specific methods designed for general label noise exhibit clear limitations under SPML conditions. The following subsections detail dataset- and scenario-specific observations.

1) *reBEN-Random*: Table III presents the results on the reBEN dataset under *Random* SPML noise. AdaGC delivers the strongest overall performance, achieving the highest mAP, OA, and mF1, together with the best coverage and rankloss scores. Although not optimal in mprecision or mrecall individually, it provides the most effective precision–recall trade-off, as reflected by its mF1. General label-noise and PUL methods perform well in this setting, often surpassing SPML-specific approaches. WAN remains particularly competitive among baselines. Within RS-specific methods, RCML offers noticeable improvements compared to baselines, whereas LCR contributes little due to its fixed class-correlation assumptions. Compared with GT training, AdaGC closely approaches the full-label upper bound, especially in mF1. Compared to IUN, AdaGC attains slightly lower mAP but higher mF1. This highlights the importance of incorporating pseudo-labeling or label-correction mechanisms to recover missing labels and avoid confirmation bias.

2) *reBEN-Dominant*: *Random* SPML provides a simplified single-positive noise setting, whereas *Dominant* SPML is a more practical scenario driven by the visually dominant

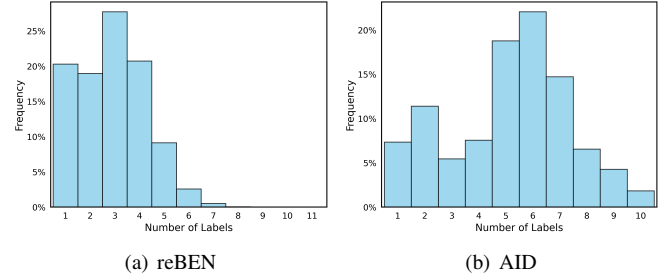


Fig. 4. Histograms of the number of GT labels per image in the training sets.

class in each image, resulting in systematic omission of non-dominant classes. This significantly increases task difficulty, as reflected in Table IV, where all methods exhibit lower absolute performance compared with Table III. Despite this challenge, AdaGC remains the strongest method, achieving the best mAP, mF1, coverage, and rankloss. In contrast, most competing approaches fail to surpass the WAN and EPR baselines. WAN obtains the second-best mAP and outperforms all SPML-specific methods in mF1. LL-based methods and Dist-PU offer additional gains over WAN in mF1, yet still fall short of EPR. Thanks to its cardinality regularization, EPR effectively mitigates the strong bias induced by *Dominant* SPML, yielding competitive mF1 despite its low mAP. RCML remains relatively strong but continues to underperform the proposed AdaGC.

3) *AID-Random*: Table V reports the results on the AID dataset under *Random* SPML noise. Owing to ImageNet pre-training and richer spatial information, this dataset yields higher absolute performance than reBEN, despite larger flip

TABLE VI

TEST PERFORMANCE COMPARISON OF DIFFERENT METHODS ON THE AID-MANUAL DATASET. THE BEST AVERAGE METRIC VALUES ARE REPORTED IN BOLD, SECOND BESTS ARE IN ITALIC. THE RELATED STANDARD DEVIATIONS ARE REPORTED IN BRACKETS

		mAP (%) ↑	Coverage ↓	Rankloss (%) ↓	OA (%) ↑	mF1 (%) ↑	mprecision (%) ↑	mrecall (%) ↑
Ground-truth Training	GT w/ BCE	89.01 (0.32)	5.834 (0.011)	1.657 (0.061)	94.29 (0.19)	83.12 (0.66)	88.87 (0.38)	79.58 (1.28)
	IUN	82.71 (0.60)	6.638 (0.085)	3.068 (0.191)	91.47 (0.16)	74.83 (0.42)	94.18 (3.95)	65.53 (0.89)
Baseline Methods	AN	67.66 (0.73)	8.589 (0.140)	11.276 (0.283)	71.30 (0.08)	29.01 (0.59)	83.94 (1.69)	18.83 (0.56)
	AN-LS	66.75 (0.62)	11.556 (0.061)	23.300 (0.640)	71.34 (0.17)	28.41 (1.81)	84.61 (1.94)	18.32 (1.19)
	WAN	70.28 (0.50)	7.721 (0.103)	8.364 (0.276)	75.35 (0.29)	45.28 (1.77)	88.30 (4.71)	32.21 (1.68)
	EPR ^a	71.92 (1.36)	7.251 (0.118)	8.766 (0.358)	84.89 (0.50)	71.30 (1.06)	63.86 (1.49)	83.84 (0.56)
General Label Noise Methods	ELR	76.99 (0.51)	7.278 (0.107)	5.353 (0.232)	88.26 (0.31)	69.09 (0.63)	77.43 (0.47)	68.55 (1.33)
	LL-Cp	69.65 (0.54)	7.854 (0.073)	8.982 (0.470)	70.87 (0.07)	23.14 (0.23)	80.08 (3.81)	14.94 (0.28)
	LL-Ct	72.46 (0.11)	7.564 (0.104)	7.788 (0.525)	76.04 (0.12)	42.70 (0.69)	85.52 (2.13)	30.93 (0.24)
	LL-R	73.89 (0.29)	7.743 (0.007)	6.560 (0.094)	83.95 (0.05)	63.51 (1.55)	80.53 (1.29)	54.60 (1.90)
PUL Methods	BoostLU	71.35 (1.77)	8.441 (0.061)	8.976 (0.247)	75.61 (0.06)	42.58 (0.40)	83.31 (6.37)	31.62 (0.56)
	Dist-PU ^a	74.90 (1.88)	6.574 (0.021)	3.652 (0.085)	90.23 (0.34)	66.77 (1.16)	80.98 (0.23)	62.70 (1.32)
SPML Methods	ROLE	64.36 (1.99)	13.253 (0.101)	17.429 (0.973)	76.41 (0.64)	49.11 (2.03)	86.08 (4.40)	36.30 (2.01)
	GR	67.18 (0.65)	11.042 (0.191)	21.481 (0.353)	71.63 (0.14)	29.88 (1.34)	86.64 (4.63)	19.93 (1.17)
	LAC	65.80 (0.81)	7.878 (0.066)	9.395 (0.259)	72.64 (0.16)	31.72 (1.58)	80.81 (4.74)	21.03 (1.04)
	MIME	65.39 (1.07)	7.240 (0.147)	6.333 (0.424)	73.10 (0.14)	32.62 (0.89)	84.73 (6.70)	21.70 (0.65)
RS-specific Methods	RCML	72.87 (0.57)	7.453 (0.019)	7.393 (0.266)	80.46 (1.44)	52.99 (3.67)	85.83 (2.34)	43.08 (5.79)
	LCR	66.61 (0.96)	8.322 (0.078)	10.669 (0.472)	71.79 (0.22)	31.83 (1.46)	85.52 (1.57)	21.03 (1.02)
Proposed	AdaGC	79.07 (0.91)	<i>6.673 (0.103)</i>	<i>4.620 (0.558)</i>	<i>82.66 (1.01)</i>	71.95 (0.94)	68.25 (2.35)	82.61 (1.28)

^a EPR and Dist-PU use additional a-priori information, which is assumed unknown in all other approaches.

rates β_c . AdaGC shows the best performance across all metrics. It achieves the highest mAP and the second-best mF1, mrecall, coverage, and rankloss scores. Dist-PU also shows excellent results, matching AdaGC in mF1 while achieving the best OA, coverage, and rankloss. Meanwhile, EPR reaches the highest mF1 overall. The strong outcomes of Dist-PU and EPR are largely attributable to their use of prior information about the underlying GT label distributions, which is not available to AdaGC. Dist-PU assumes knowledge of class-prior distributions and aligns predicted label frequencies accordingly, whereas EPR relies on the expected number of positive labels per image. These priors are particularly beneficial for AID, which contains more labels per image on average (Fig. 4). As a result, EPR achieves the highest mrecall, although this comes at the cost of the lowest mprecision, reflecting its tendency to overestimate positives. Still, RCML achieves some comparable results to other considered methods, whereas the improvement brought by LCR remains limited.

4) *AID-Manual*: Table VI reports the results on the AID dataset using *Manual* SPML labels to further evaluate AdaGC’s practical effectiveness. Benefiting from human-induced bias in single-positive labels, most methods achieve higher performance compared with *AID-Random*. In this setting, AdaGC remains highly effective, getting the highest mAP and mF1, and ranking among the top methods across nearly all metrics. Dist-PU again achieves the best OA, coverage, and rankloss by leveraging extra prior information. RS-specific methods show similar trends as before. RCML provides moderate improvements over other SPML or label-noise baselines, while LCR contributes little due to the fixed class-correlation assumptions. Overall, the AID-Manual re-

sults confirm that higher-quality single-positive labels enhance learning, and AdaGC consistently delivers robust performance without relying on additional priors.

D. Ablation Experiments

We conduct ablation experiments on reBEN under both types of label noise to evaluate the effectiveness of individual components in AdaGC. Without making specific claims, we report the accuracies of the teacher models below.

1) *Impact of Early Learning Detection*: We evaluate the effectiveness of early learning detection for adaptively triggering GC by comparing AdaGC with variants that use manually predefined trigger points. Fig. 5 plots their validation accuracies (wrt GT labels) over training time. The proposed adaptive detection strategy successfully activates GC at an appropriate point, resulting in the most significant performance improvements. This demonstrates that the timing of GC activation is essential for model convergence stability. In contrast, triggering GC too early or too late leads to suboptimal results. Notably, activating GC too late leads to even worse performance, highlighting the detrimental effect of overfitting to label noise. Furthermore, we report their final test accuracies in Table VII. AdaGC achieves competitive or comparable mAP and mF1 scores compared to those obtained using fixed warm-up lengths, indicating the robustness of the proposed early learning detection strategy.

We demonstrate the necessity of using the teacher model for early learning detection by comparing the smoothness of noisy validation accuracies from the student and teacher models in Fig. 6. Although both models exhibit similar overall trends, the teacher model produces noticeably smoother accuracy curves.

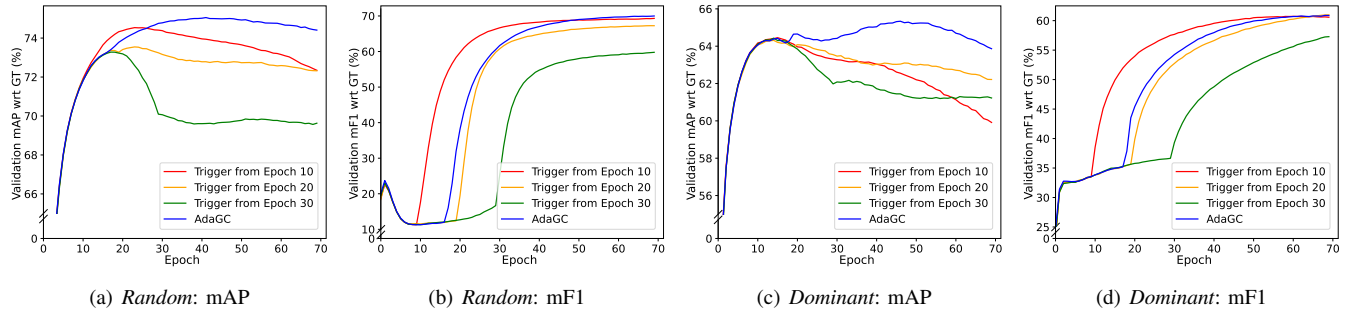


Fig. 5. Validation accuracies (mAP and mF1) over training epochs obtained with predefined warm-up lengths (10, 20, 30) and our proposed early learning detection strategy (AdaGC).

TABLE VII

ACCURACIES (%) ON THE TEST SET OBTAINED WITH DIFFERENT GC TRIGGER SETTINGS AFTER 70 EPOCHS

	Random		Dominant	
	mAP ↑	mF1 ↑	mAP ↑	mF1 ↑
AdaGC (after \sim 17 epochs)	68.18	64.65	60.22	58.78
Trigger after 10 epochs	65.78	64.06	57.16	58.58
Trigger after 20 epochs	65.87	62.39	59.35	59.28
Trigger after 30 epochs	63.18	54.77	58.62	55.71

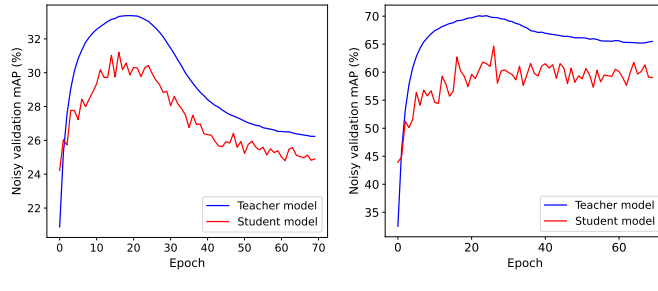


Fig. 6. Noisy validation mAP (with respect to noisy labels) versus training time (epoch) obtained by AN on the reBEN dataset.

This stability makes it more suitable for reliable early learning detection. In contrast, detections based on the student model are more prone to local maxima, resulting in unstable and suboptimal outcomes.

2) *Effect of the Dual-EMA Mechanism:* We investigate the effect of the proposed dual-EMA mechanism by comparing it with single-EMA and no-EMA settings, as shown in Table VIII. The dual-EMA strategy consistently achieves the most robust performance by striking a balance between stability and adaptability. In contrast, the single-EMA and no-EMA variants exhibit suboptimal results, particularly when the EMA smoothing on student predictions is removed. In both *Random* and *Dominant* noise settings, the EMA-smoothed student predictions are more stable than the teacher-only ones, owing to the teacher's slower update rate. Nevertheless, without EMA smoothing (no-EMA), the student's raw predictions tend to amplify errors, resulting in additional performance degradation. This trend is further confirmed in Fig. 7, where pseudo-label quality is shown to have a strong

TABLE VIII

TEST SET ACCURACIES (%) OBTAINED USING DIFFERENT PSEUDO-LABEL GENERATION STRATEGIES, WHERE T, S, AND S' DENOTE TEACHER MODEL PREDICTIONS, EMA-SMOOTHED STUDENT MODEL PREDICTIONS, AND STUDENT MODEL PREDICTIONS WITHOUT EMA, RESPECTIVELY

EMA Settings	Random		Dominant		
	mAP ↑	mF1 ↑	mAP ↑	mF1 ↑	
dual	AdaGC	68.18	64.65	60.22	58.78
	Only T ($\gamma = 1$)	61.74	63.49	42.01	46.40
single	Only S ($\gamma = 0$)	67.93	61.52	60.11	57.42
	T+S' ($\gamma = 0.5$)	53.78	61.94	27.50	35.71
no	Only S' ($\gamma = 0$)	49.30	52.89	16.41	25.24

TABLE IX
TEST ACCURACIES (%) OBTAINED WITH AND WITHOUT MIXUP

	Random		Dominant	
	mAP ↑	mF1 ↑	mAP ↑	mF1 ↑
AdaGC	68.18	64.65	60.22	58.78
w/o Mixup	66.00	62.08	59.05	59.19

impact on AdaGC's performance. As the pseudo-label quality deteriorates, performance drops markedly, especially for the teacher-only and no-EMA cases. The dual-EMA mechanism mitigates these issues by smoothing student predictions and integrating teacher outputs, thereby generating more reliable pseudo labels. Considering the varying update dynamics of the student and teacher models during training, a more adaptive combination strategy beyond the current half-half scheme is expected to enhance robustness, which we leave for future exploration.

3) *Role of Mixup:* We then investigate the effect of Mixup under both *Random* and *Dominant* noise settings. As shown in Table IX, removing Mixup consistently reduces performance, particularly in the *Random* case, with about a 2% drop in mAP and mF1. This indicates that Mixup enhances generalization by enforcing smoother decision boundaries. It can complement the GC mechanism in improving the robustness of AdaGC.

V. CONCLUSION

In this work, we have presented AdaGC, a novel and generalizable framework for SPML tailored to RS imagery, which addresses overfitting to false negatives via a gradient calibration mechanism. To ensure its operational effectiveness,

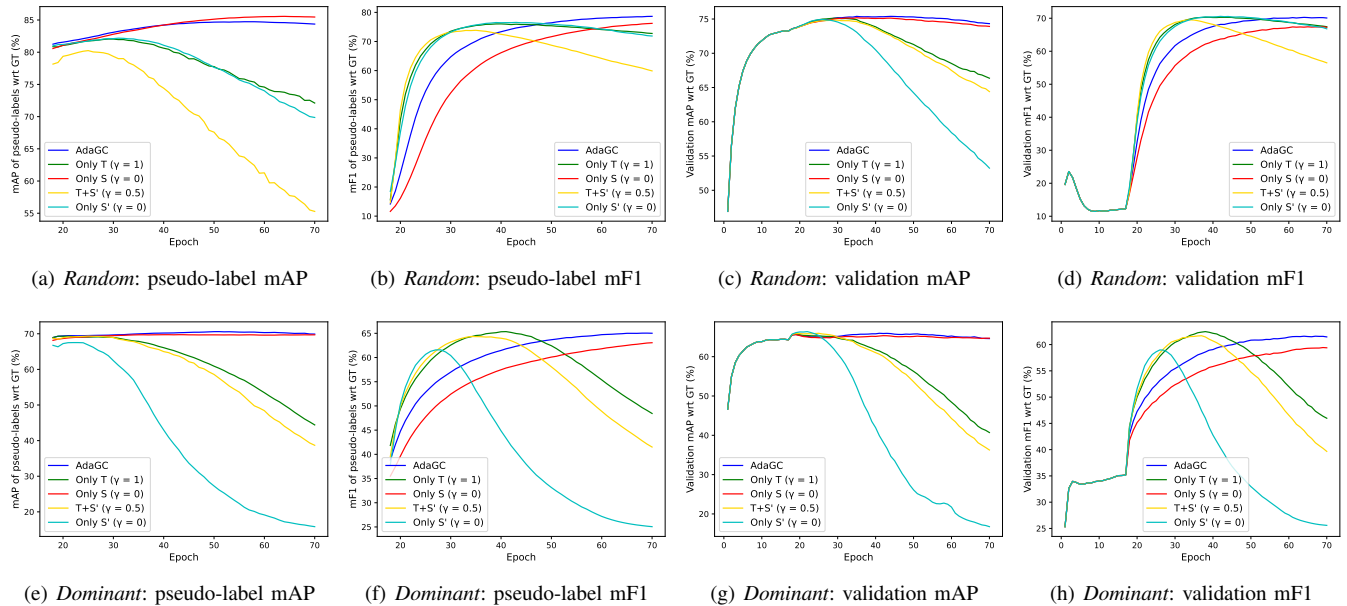


Fig. 7. Pseudo-label quality (a), (b), (e), (f) and AdaGC validation accuracies (mAP and mF1) (c), (d), (g), (h) over training epochs using different pseudo-label generation strategies, where T, S, and S' denote teacher model predictions, EMA-smoothed student model predictions, and student model predictions without EMA, respectively. (a)-(d) Random single-positive labels case. (e)-(h) Dominant single-positive labels case.

we introduce a simple yet theoretically grounded indicator to adaptively activate GC when it detects the end of early learning during an initial warm-up stage. In addition, a dual-EMA module is introduced to produce robust pseudo-labels that support the GC process, along with Mixup to further boost the robustness of training.

Extensive experiments on two benchmark RS datasets under two single-positive realistic label noise simulation settings, *Random* and *Dominant*, demonstrate the effectiveness and robustness of AdaGC. AdaGC consistently outperforms existing SPML baselines across different scenarios. Our work fills a critical gap in the literature, where SPML remains largely unexplored in the RS domain. While AdaGC performs well in most settings, it shows relative limitations under the dominant single-positive label noise condition. As this scenario is common in many real-world annotation practices, future work will focus on enhancing AdaGC's performance under such conditions, further advancing scalable and reliable multi-label learning in RS.

REFERENCES

- [1] T. Zhao *et al.*, “Artificial intelligence for geoscience: Progress, challenges and perspectives,” *The Innov.*, vol. 5, no. 5, Sep. 2024, Art. no. 100691.
- [2] X. X. Zhu *et al.*, “On the Foundations of Earth and Climate Foundation Models,” 2024, *arXiv:2405.04285*.
- [3] M. Mahmood, A. Shahzad, B. Zafar, A. Shabbir, and N. Ali, “Remote Sensing Image Classification: A Comprehensive Review and Applications,” *Math. Problems Eng.*, vol. 2022, no. 1, Aug. 2022, Art. no. 5880959.
- [4] I. Dimitrovski, I. Kitanovski, D. Kocev, and N. Simidjievski, “Current trends in deep learning for Earth Observation: An open-source benchmark arena for image classification,” *ISPRS J. Photogrammetry Remote Sens.*, vol. 197, pp. 18–35, Mar. 2023.
- [5] L. He, J. Li, C. Liu, and S. Li, “Recent Advances on Spectral–Spatial Hyperspectral Image Classification: An Overview and New Guidelines,” *IEEE Trans. Geosci. Remote Sens.*, vol. 56, no. 3, pp. 1579–1597, Mar. 2018.
- [6] Y. Hua, L. Mou, and X. X. Zhu, “Recurrently exploring class-wise attention in a hybrid convolutional and bidirectional LSTM network for multi-label aerial image classification,” *ISPRS J. Photogrammetry Remote Sens.*, vol. 149, pp. 188–199, Mar. 2019.
- [7] G. Sumbul and B. Demir, “A Deep Multi-Attention Driven Approach for Multi-Label Remote Sensing Image Classification,” *IEEE Access*, vol. 8, pp. 95 934–95 946, May 2020.
- [8] T. Burgert, M. Ravanbakhsh, and B. Demir, “On the Effects of Different Types of Label Noise in Multi-Label Remote Sensing Image Classification,” *IEEE Trans. Geosci. Remote Sens.*, vol. 60, Dec. 2022, Art. no. 5413713.
- [9] X. X. Zhu *et al.*, “Deep Learning in Remote Sensing: A Comprehensive Review and List of Resources,” *IEEE Geosci. Remote Sens. Mag.*, vol. 5, no. 4, pp. 8–36, Dec. 2017.
- [10] E. Cole, O. Mac Aodha, T. Lorieul, P. Perona, D. Morris, and N. Jovic, “Multi-Label Learning From Single Positive Labels,” in *Proc. IEEE Conf. Comput. Vis. Pattern Recog.*, Nashville, TN, USA, Jun. 2021, pp. 933–942.
- [11] Y. Hua, L. Mou, and X. X. Zhu, “Relation Network for Multilabel Aerial Image Classification,” *IEEE Trans. Geosci. Remote Sens.*, vol. 58, no. 7, pp. 4558–4572, Jul. 2020.
- [12] K. N. Clasen, L. Hackel, T. Burgert, G. Sumbul, B. Demir, and V. Markl, “reBEN: Refined BigEarthNet Dataset for Remote Sensing Image Analysis,” May 2025, *arXiv:2407.03653*.
- [13] H. Zhang, M. Cisse, Y. N. Dauphin, and D. Lopez-Paz, “mixup: Beyond Empirical Risk Minimization,” in *Proc. Int. Conf. Learn. Representations*, Vancouver, Canada, Apr./May 2018.
- [14] Y. Kim, J. M. Kim, Z. Akata, and J. Lee, “Large Loss Matters in Weakly Supervised Multi-Label Classification,” in *Proc. IEEE Conf. Comput. Vis. Pattern Recog.*, New Orleans, LA, USA, Jun. 2022, pp. 14 156–14 165.
- [15] M.-K. Xie, J. Xiao, and S.-J. Huang, “Label-Aware Global Consistency for Multi-Label Learning with Single Positive Labels,” in *Adv. Neural Inform. Process. Syst.*, vol. 35, Louisiana, LA, USA, Nov./Dec. 2022, pp. 18 430–18 441.
- [16] Y. Chen *et al.*, “Boosting single positive multi-label classification with generalized robust loss,” in *Proc. Int. Joint Conf. Artif. Intell.*, Jeju, Korea, Aug. 2024, pp. 3825–3833.
- [17] Y. Kim, J. M. Kim, J. Jeong, C. Schmid, Z. Akata, and J. Lee, “Bridging the Gap Between Model Explanations in Partially Annotated Multi-Label Classification,” in *Proc. IEEE Conf. Comput. Vis. Pattern Recog.*, Vancouver, Canada, Jun. 2023, pp. 3408–3417.
- [18] B. Liu, N. Xu, J. Lv, and X. Geng, “Revisiting Pseudo-Label for Single-

Positive Multi-Label Learning," in *Proc. Int. Conf. Mach. Learn.*, vol. 202, Jul. 2023, pp. 22249–22265.

[19] S. Liu, J. Niles-Weed, N. Razavian, and C. Fernandez-Granda, "Early-Learning Regularization Prevents Memorization of Noisy Labels," in *Advances in Neural Information Processing Systems*, vol. 33. Curran Associates, Inc., 2020, pp. 20331–20342. [Online]. Available: <https://proceedings.neurips.cc/paper/2020/hash/ea89621bee7c88b2c5be6681c8ef4906-Abstract.html>

[20] A. Zeggada, F. Melgani, and Y. Bazi, "A Deep Learning Approach to UAV Image Multilabeling," *IEEE Geosci. Remote Sens. Lett.*, vol. 14, no. 5, pp. 694–698, May 2017.

[21] S. Koda, A. Zeggada, F. Melgani, and R. Nishii, "Spatial and Structured SVM for Multilabel Image Classification," *IEEE Trans. Geosci. Remote Sens.*, vol. 56, no. 10, pp. 5948–5960, Oct. 2018.

[22] O. Russakovsky *et al.*, "ImageNet Large Scale Visual Recognition Challenge," *Int. J. Comput. Vis.*, vol. 115, no. 3, pp. 211–252, Apr. 2015.

[23] R. Stivaktakis, G. Tsagkatakis, and P. Tsakalides, "Deep Learning for Multilabel Land Cover Scene Categorization Using Data Augmentation," *IEEE Geosci. Remote Sens. Lett.*, vol. 16, no. 7, pp. 1031–1035, Jul. 2019.

[24] A. Alshehri, Y. Bazi, N. Ammour, H. Almubarak, and N. Alajlan, "Deep Attention Neural Network for Multi-Label Classification in Unmanned Aerial Vehicle Imagery," *IEEE Access*, vol. 7, pp. 119873–119880, Aug. 2019.

[25] M.-K. Xie and S.-J. Huang, "CCMN: A General Framework for Learning With Class-Conditional Multi-Label Noise," *IEEE Trans. Pattern Anal. Mach. Intell.*, vol. 45, no. 1, pp. 154–166, Jan. 2023.

[26] M. C. du Plessis, G. Niu, and M. Sugiyama, "Analysis of Learning from Positive and Unlabeled Data," in *Adv. Neural Inform. Process. Syst.*, vol. 27, Montréal, Canada, Dec. 2014, pp. 703–711.

[27] G. Niu, M. C. du Plessis, T. Sakai, Y. Ma, and M. Sugiyama, "Theoretical Comparisons of Positive-Unlabeled Learning against Positive-Negative Learning," in *Adv. Neural Inform. Process. Syst.*, vol. 29, Barcelona, Spain, Dec. 2016, pp. 1199–1207.

[28] J. Bekker and J. Davis, "Learning from positive and unlabeled data: A survey," *Mach. Learn.*, vol. 109, no. 4, pp. 719–760, Apr. 2020.

[29] G. Perantoni and L. Bruzzone, "Robust Training of Deep Neural Networks with Weakly Labelled Data," in *Signal and Image Processing for Remote Sensing*, C. H. Chen, Ed. Boca Raton, FL, USA: CRC Press, 2024, ch. 14, pp. 256–279.

[30] P. Li *et al.*, "Robust deep neural networks for road extraction from remote sensing images," *IEEE Trans. Geosci. Remote Sens.*, vol. 59, no. 7, pp. 6182–6197, Jul. 2021.

[31] R. Zhang *et al.*, "Remote Sensing Image Scene Classification with Noisy Label Distillation," *Remote Sens.*, vol. 12, no. 15, Jul. 2020, Art. no. 2376.

[32] S. Liu, J. Niles-Weed, N. Razavian, and C. Fernandez-Granda, "Early-Learning Regularization Prevents Memorization of Noisy Labels," in *Adv. Neural Inform. Process. Syst.*, vol. 33, Virtual, Dec. 2020, pp. 20331–20342.

[33] C. Paris and L. Bruzzone, "A Novel Approach to the Unsupervised Extraction of Reliable Training Samples From Thematic Products," *IEEE Trans. Geosci. Remote Sens.*, vol. 59, no. 3, pp. 1930–1948, Mar. 2021.

[34] A. K. Aksoy, M. Ravanbakhsh, T. Kreuziger, and B. Demir, "A Consensual Collaborative Learning Method for Remote Sensing Image Classification Under Noisy Multi-Labels," in *Proc. IEEE Int. Conf. Image Process.*, Anchorage, AK, USA, Sep. 2021, pp. 3842–3846.

[35] A. K. Aksoy, M. Ravanbakhsh, and B. Demir, "Multi-Label Noise Robust Collaborative Learning for Remote Sensing Image Classification," *IEEE Trans. Neural Netw. Learn. Syst.*, vol. 35, no. 5, pp. 6438–6451, May 2024.

[36] Y. Hua, S. Lobry, L. Mou, D. Tuia, and X. X. Zhu, "Learning Multi-Label Aerial Image Classification Under Label Noise: A Regularization Approach Using Word Embeddings," in *Proc. IEEE Int. Geosci. Remote Sens. Symp.*, Waikoloa, HI, USA, Sep./Oct. 2020, pp. 525–528.

[37] A. A. Alemi, I. Fischer, J. V. Dillon, and K. Murphy, "Deep Variational Information Bottleneck," in *Proc. Int. Conf. Learn. Representations*, Toulon, France, Apr. 2017.

[38] Y. Zhao, Q. Xu, Y. Jiang, P. Wen, and Q. Huang, "Dist-PU: Positive-Unlabeled Learning From a Label Distribution Perspective," in *Proc. IEEE Conf. Comput. Vis. Pattern Recog.*, New Orleans, LA, USA, Jun. 2022, pp. 14461–14470.

[39] C. Liu, C. M. Albrecht, Y. Wang, Q. Li, and X. X. Zhu, "AOI2: Online Correction of Object Labels for Deep Learning With Incomplete Annotation in Remote Sensing Image Segmentation," *IEEE Trans. Geosci. Remote Sens.*, vol. 62, Mar. 2024, Art. no. 5613917.

[40] D. Arpit *et al.*, "A closer look at memorization in deep networks," in *Proc. Int. Conf. Mach. Learn.*, Sydney, Australia, Aug. 2017, pp. 233–242.

[41] C. Zhang, S. Bengio, M. Hardt, B. Recht, and O. Vinyals, "Understanding deep learning (still) requires rethinking generalization," *Commun. ACM*, vol. 64, no. 3, pp. 107–115, Feb. 2021.

[42] G. Perantoni and L. Bruzzone, "A Novel Technique for Robust Training of Deep Networks With Multisource Weak Labeled Remote Sensing Data," *IEEE Trans. Geosci. Remote Sens.*, vol. 60, 2022, Art. no. 5402915.

[43] A. Tarvainen and H. Valpola, "Mean teachers are better role models: Weight-averaged consistency targets improve semi-supervised deep learning results," in *Adv. Neural Inform. Process. Syst.*, vol. 30, Long Beach, CA, USA, Dec. 2017, pp. 1195–1204.

[44] G. Sumbul, M. Charfuelan, B. Demir, and V. Markl, "Bigearthnet: A Large-Scale Benchmark Archive for Remote Sensing Image Understanding," in *Proc. IEEE Int. Geosci. Remote Sens. Symp.*, Yokohama, Japan, 2019, pp. 5901–5904.

[45] G. Sumbul *et al.*, "BigEarthNet-MM: A Large-Scale, Multimodal, Multilabel Benchmark Archive for Remote Sensing Image Classification and Retrieval [Software and Data Sets]," *IEEE Geosci. Remote Sens. Mag.*, vol. 9, no. 3, pp. 174–180, Sep. 2021.

[46] G.-S. Xia *et al.*, "AID: A Benchmark Data Set for Performance Evaluation of Aerial Scene Classification," *IEEE Trans. Geosci. Remote Sens.*, vol. 55, no. 7, pp. 3965–3981, Jul. 2017.

[47] F. Liu *et al.*, "RemoteCLIP: A Vision Language Foundation Model for Remote Sensing," *IEEE Trans. Geosci. Remote Sens.*, vol. 62, Apr. 2024, Art. no. 5622216.